Materials Science & Engineering A 820 (2021) 141557

Contents lists available at ScienceDirect

Materials Science & Engineering A

journal homepage: www.elsevier.com/locate/msea

Effect of pre-deformation on age-hardening behaviors in an Al-Mg-Cu alloy

Xuanliang Chen [a,*], Daehan Kim [b], Minho O [a], Calin D. Marioara [c], Sigmund J. Andersen [c], Adrian Lervik [d], Randi Holmestad [d], Equo Kobayashi [a]

[a] Department of Materials Science and Engineering, Tokyo Institute of Technology, 2-12-1-S8-18, Ookayama, Meguro-ku, Tokyo, 152-8552, Japan
[b] Carbon & Light Materials Application Group, Korea Institute of Industrial Technology, 222 Palbok-ro, Jeonju-si, 54896, South Korea
[c] Materials and Nanotechnology, SINTEF Industry, Høgskoleringen 5, N-7465, Trondheim, Norway
[d] Department of Physics, Norwegian University of Science and Technology, Høgskoleringen 5, N-7491, Trondheim, Norway

ARTICLE INFO

Keywords:
Aluminum alloys
Plasticity methods
Phase transformation
Hardness
Thermal analysis
Electron microscopy

ABSTRACT

The effects of 3%–50% pre-deformation following solution heat treatment on the age hardening of an Al-3Mg-1Cu alloy have been investigated by Vickers microhardness measurement, tensile tests, differential scanning calorimetry, scanning electron microscopy, and transmission electron microscopy. Pre-deformation has a strong effect on subsequent age-hardening behavior. The precipitation was accelerated, hardness peaks appeared earlier, formation of clusters was inhibited, and a larger fraction of precipitates was observed along the dislocation lines. The contribution of the precipitates to the hardness was evaluated by dissolution tests. It was found that pre-deformation followed by artificial aging resulted in a good strength-elongation balance. The results are significant for the development of combined mechanical deformation and heat treatment processes.

1. Introduction

Aluminum alloys with Cu and Mg as the main alloying elements are important lightweight structural materials for aerospace and automotive applications [1,2]. This is due to their superior mechanical properties developed by a complex heat treatment process that includes solution heat treatment (SHT) followed by aging heat treatment. SHT takes place at a temperature above the solvus line, where the solute elements dissolve in the Al lattice. A subsequent fast cooling to a low temperature, typically room-temperature (RT), produces a supersaturated solid solution (SSSS) in which the alloying elements are bound to the Al face-centered cubic (FCC) lattice positions. The same applies for the vacancies: The high natural concentration of vacancies at the SHT temperature is quenched into the RT state. These quenched-in vacancies [3] mediate solute transport (diffusion) in the lattice and are responsible for the initial formation of solute clusters. They may also join to form low-energy vacancy orderings, such as dislocation loops [4]. After SHT, the alloy is heated to an intermediate temperature (approximately 443 K) in a process known as artificial aging (AA). This leads to precipitation, where the supersaturated and well-distributed Cu and Mg solute atoms are ordered into nanoscale precipitates that are partly coherent with the aluminum host matrix. The resulting chemical differences create obstacles for the movement of dislocations during deformation, which greatly increase the strength of the material. Depending on the temperature and holding time, the precipitates grow, dissolve, nucleate, and transform into new forms until the most stable phase is reached. The sequence of precipitation leading to the stable S phases can be summarized as [5–9]:

$$\text{SSSS} \rightarrow \text{Cu/Mg clusters} \rightarrow \text{GPB zones} \rightarrow \text{S phases} \quad (1)$$

Here, SSSS is the state in which the Al lattice is a supersaturated solid solution. Clusters are local aggregates of solute atoms and there are often vacancies at the Al positions in the FCC structure. The Guinier–Preston–Bagaryatsky (GPB) zones are considered as fine-scaled solute-enriched regions of longer order where both vacancies and interstitials can deviate from the host lattice. The S phases are equilibrium precipitates with the composition Al_2CuMg, which are, in principle, stable phases that can exist independent of the Al.

Available literature rarely makes a clear distinction between the Cu/Mg clusters and GPB zones. We define GPB zones as those possessing a definite structure, whereas clusters do not have such a structure. Several types of GPB zones exist. Some of the examples of this system are the frequently reported $GPB^{(n)}$ [10–12], GPB-T [13], and GPBX [9,14] zones. The S phase is related to S′ and S′′ [8,15,16]. The S″ phase is considered a GPB zone [8], while S', due to coherency, is a slightly strained version of the equilibrium S phase [15]. They are collectively

* Corresponding author.
E-mail address: chen.x.af@m.titech.ac.jp (X. Chen).

https://doi.org/10.1016/j.msea.2021.141557
Received 27 February 2021; Received in revised form 24 April 2021; Accepted 2 June 2021
Available online 10 June 2021

denoted as S phases as their structures are similar, although with lattice parameters that can change during aging [15]. The S phases are also classified into two different categories based on their morphology and orientation relationship with the Al matrix: the $<012>_{Al}$ oriented lath-shaped S-I phase and the $<014>_{Al}$ orientated rod-shaped S-II phase [9,17–19].

Age-hardening behavior in Al-Cu-Mg alloys has been investigated by several groups [20–24]. A characteristic feature of these alloys is the rapid age-hardening phenomenon. This refers to an initial rapid increase in hardness during aging, which may be attributed to the formation of solute clusters [6,22–24] or GPB zones [10,12,25]. However, there are no unified interpretations. A second feature during aging is the presence of a hardness plateau after the initial increase, where the hardness remains constant for a long time. A second hardening stage occurred after the plateau ended at the peak hardness value. This is followed by the conventional over-aging stage, where the hardness decreases owing to the coarsening of precipitates and less coherency strain.

Although the conventional age-hardening behavior is well understood, materials (or components) sometimes need to undergo processing before heat treatment. For example, car body panel sheets are often press-formed before the paint is subjected to baking which involves the heat treatment (443 K for 20–30 min) of the sheets after painting, but without a solution heat treatment in between. This implies that the precipitation takes place in a deformed material. Therefore, the pre-deformation has a significant effect on subsequent precipitation heat treatment. It has been investigated in Al-Cu alloys [26,27], but Al-Mg-Cu alloys with high Mg/Cu ratios have not been the subject of wide study.

In this work, cold rolling (CR) of the Al-Mg-Cu alloy is performed before aging to investigate the effect of pre-deformation on the aging behavior. Considering that the local deformation of the different parts may be different during the press-forming process, a wide range of reduction rates (from 3 to 50%) were selected. This ensures that the obtained results have a broader range, which is significant for both shape and process design. The microstructures and mechanical properties of the pre-deformed aged sample are reported and discussed. In addition, the hardness contributions of the GPB zones and S phases under various conditions are evaluated.

2. Materials and methods

Table 1 lists the chemical composition of the high-purity Al-3Mg-1Cu alloy used in this study. The heat treatment and cold rolling processes are illustrated in Fig. 1(a) and (b), respectively. Samples of size 10 × 10 × 1.2 mm^3 were solution heat-treated in a salt bath at 793 K for 1 h, followed by quenching in iced water, where it was held for 1 min. The quenched samples were subsequently cold-rolled at RT at reduction rates of 0%, 3%, 7%, 10%, 25%, and 50%. The rolling ratio was determined by measuring the reduction in sheet thickness. Isothermal aging was carried out in oil baths at RT, 393 K, and 443 K for the selected holding times. The as-quenched and as-rolled conditions are abbreviated as “AQ” and “AR,” respectively. The samples with and without pre-deformation are called “base” and “CR” samples, respectively. Dissolution heat treatment was performed in salt baths for 2 min at the corresponding dissolution peak temperatures of GPB zones to determine the contribution of the precipitates to hardness.

The micro-Vickers hardness was measured at RT by applying a load of 200 g for 15 s in a Matsuzawa MMT-X micro-hardness tester. Every reported hardness value is the average of five out of a set of seven hardness data points (excluding the two extremal values).

Table 1
Chemical composition of the investigated Al alloy in wt.% and at.%.

Element	Mg	Cu	Si	Fe	Al
wt.%	3.04	1.01	0.01	0.01	Bal.
at.%	3.38	0.43	0.01	0.005	Bal.

Differential scanning calorimetry (DSC) tests were carried out in an argon atmosphere in a Rigaku DSC8230 instrument using 40 mg of pure Al (99.99 %) as a reference, at a heating rate of 10 K/min. The temperature range for the DSC measurements (223–773 K) was monitored using a liquid nitrogen controller.

The samples were cold-rolled and aged prior to the tensile tests, from which flat dog-bone test specimens, as shown in Fig. 1(c), were cut out. For the tensile experiments, an Autograph AG-X plus tester manufactured by Shimadzu was used. The tests were conducted at RT at a strain rate of 6.07 × 10^{-4} s^{-1}. Three tensile specimens were tested for each condition and the results were found to be reproducible.

The tensile direction is parallel to the rolling direction. The fracture surfaces of the tensile-tested samples were observed using a field emission scanning electron microscope (FE-SEM, JEOL JSM-7200F) operated at 15 kV.

Specimens for transmission electron microscopy (TEM) were prepared from 1.2 mm sheet samples. They were reduced by grinding the samples into foils with a thickness of ~100 μm. Discs of 3 mm diameter were punched from the resulting foils and further electropolished to perforation using a Struers TenuPol-5. The electrolyte (1/3 nitric acid and 2/3 methanol) was maintained between 243 K and 253 K during electropolishing, with an applied potential of 20 V.

The precipitate microstructures were investigated by high-resolution, high-angle annular dark-field scanning TEM (HAADF-STEM) in a double Cs-corrected JEOL ARM 200CF STEM operated at 200 kV. The convergence semi-angle was set to 28 mrad, and the inner collection angle of the HAADF detector was 48 mrad. To reduce contamination, all specimens were treated for 3 min in a Fischione 1020 Plasma Cleaner prior to the TEM observations. All the presented images are along the <100>Al orientation. This is because all the precipitates are elongated along the <100>Al direction and extend mostly through the TEM specimen in the thin regions investigated, enabling good contrast.

The column contrast in the images was further enhanced by a circular bandpass mask applied to the respective fast Fourier transform (FFT), which corresponds to the removal of high spatial frequencies (noise) in the real space below 0.15 nm. An inverse FFT (IFFT) was performed on the masked area.

The HAADF-STEM technique utilizes the Z contrast arising from Rutherford scattering from the core electrons of atoms. In column-resolved images, a column having a larger average atomic number Z will have more scattering, which results in a greater brightness in the STEM image [28].

3. Results and discussion

3.1. Age-hardening behaviors

3.1.1. Age-hardening at 443 K

Fig. 2(a) shows the hardness response for aging of the investigated alloy by different treatments at 443 K. The (undeformed) base material reveals a standard four-stage change in hardness, namely a rapid initial increase, plateau, second increase to maximum hardness, and final decrease. Rapid age-hardening (R1) from 66.4 to 88.9 HV occurs within the first 60 s, followed by a plateau stage (L) that lasts for approximately 1 day. After aging for 7 to 14 days, the hardness increases again (R2) to a maximum with a peak hardness of approximately 101.0 HV. The last stage (D) is characterized by a decrease in hardness due to over-aging. It should be mentioned that R1 contributes to approximately 65% of the total increase in hardness.

The curves show that cold rolling delays the first increase in hardness, R1. Deformation effectively adds an initial incubation stage. Although more deformation generally leads to higher hardness, the two lower curves in Fig. 2(a) show that for a brief period during aging, where R1 and L meet, the delay in precipitation of the 3% CR sample results in a hardness below that of the base sample. For the 3% CR sample, R1

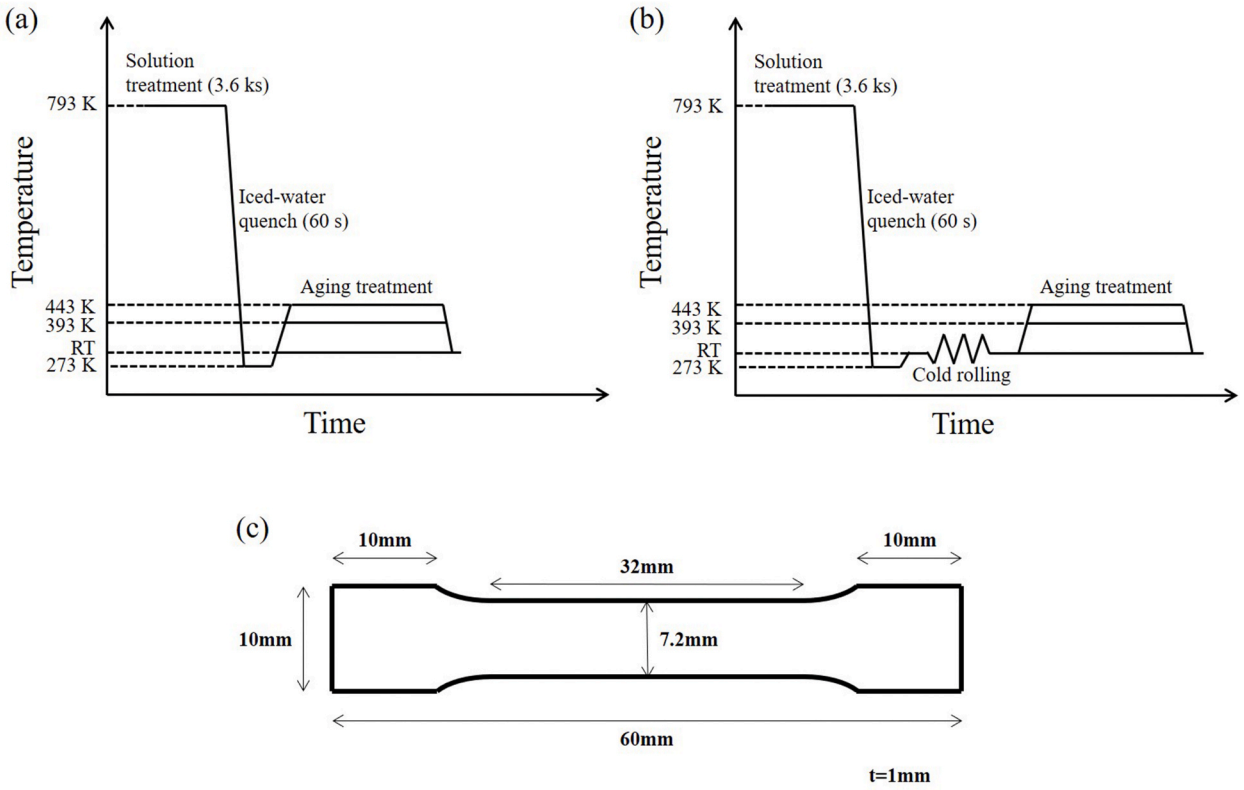

Fig. 1. Schematic of the heat treatment process with (a) standard procedure (no deformation) and (b) pre-deformation. (c) Sample geometry for tensile tests.

increases from 1 to 20 min, finally reaching a plateau level (L) above that of the base, but it starts later and ends sooner. Then, it reached a broad peak that lasted up to 1 month, after aging for 24 h. The deformation reduces the aging time for maximum hardness by a factor of approximately 10.

The curves show that the increased deformation of up to 50% shows similar age-hardening behavior and consistently higher hardness. Higher reduction rates indicated faster precipitation. Evidence of recovery behavior is obvious at the early stage for the two upper curves corresponding to the 25% and 50% CR samples. Compared with the base sample, the hardness plateaus L (and the first hardening stage R1) in samples with small reduction rates (3 to 10%) were delayed initially, but recovered again as the reduction rate increased (25 and 50%). This is discussed further in section 3.2.2. The vertical dotted line indicates the bake-hardening condition. At the position where this line intersects the curves, we see that the hardness is increased from 90.6 to 119.7 HV when 50% cold-rolling is applied.

3.1.2. *Age-hardening at 393 K and room temperature*

Artificial aging is typically performed at a temperature of 443K. However, it is important to understand aging behavior in a more general sense because precipitation depends strongly on temperature. During production, the processing steps are often separated by RT storage, also called “natural aging” (NA). Such low-temperature steps in the process often affect the precipitation. For example, different clusters have been observed to form preferentially at RT and 373 K in Al-Mg-Si alloys [29]. In this work, the age-hardening of the Al-Mg-Cu alloy at 293 K (RT) and 393 K was investigated.

The age-hardening curves for the base, 10%, and 25% CR samples aged at 393 K and RT are shown in Fig. 2 (b) and (c), respectively. For the base alloy aged at 393 K, the initial incubation stage appears before the first hardening increases the R1. The 10% and 25% CR samples behave similar to the base; however, as their kinetics are slower, they require a longer aging time to reach plateau L. The right-hand side of the curves in Fig. 2(b) shows all three samples at the L-stage after aging at 393 K for 14 days. This can be compared to 443 K in Fig. 2(a), where 14 days would allow all of them to reach the peak or the overaged stage D. As expected, Fig. 2(c) shows a much slower kinetics at RT: even after 2 years of aging, the three samples remained on the plateau. The similarity in the overall aging curve shape indicates that the same mechanisms are at play, but that the activity increases with temperature.

A main issue that curtails the large-scale application of Al alloys to automobile body panels is the requirement of long-term usage at high service temperatures (such as due to exposure to sunlight). This leads to over-aging, decreased strength, and reduced service life. The long aging time required to reach the peak hardness for the investigated Al-Mg-Cu alloy indicates good thermal stability, which can potentially address this concern.

3.2. *DSC results*

3.2.1. *DSC of the base material for various aging times*

Fig. 3(a) shows the DSC curves of the base alloy aged at 443 K for different durations. For the AQ sample, two exothermic peaks appear at 376.3 K (I) and 567.7 K (III). They signify the formation of clusters [30] and S phases [31], respectively. The exothermic peak II, expected to accompany the formation of GPB zones, was absent. The endothermic negative peaks (dips) I′ and II′ are attributed to the dissolution of the clusters and GPB zones, respectively [32], while the endothermic peak III’ represents the dissolution of the S phase.

Peak I disappears after short-term aging at 443 K, indicating that clusters have been formed and are responsible for rapid age-hardening. After aging for 12 days, peak III was strongly reduced, suggesting the formation of the S phase. Peak I′ almost disappeared while peak II’ still exists, indicating that the clusters have been dissolved and there are still GPB zones remaining to be dissolved in order to form S phases.

The exothermic peak IV is likely to correspond to a precipitate phase other than the S phase, which may form at temperatures above 443 K. It

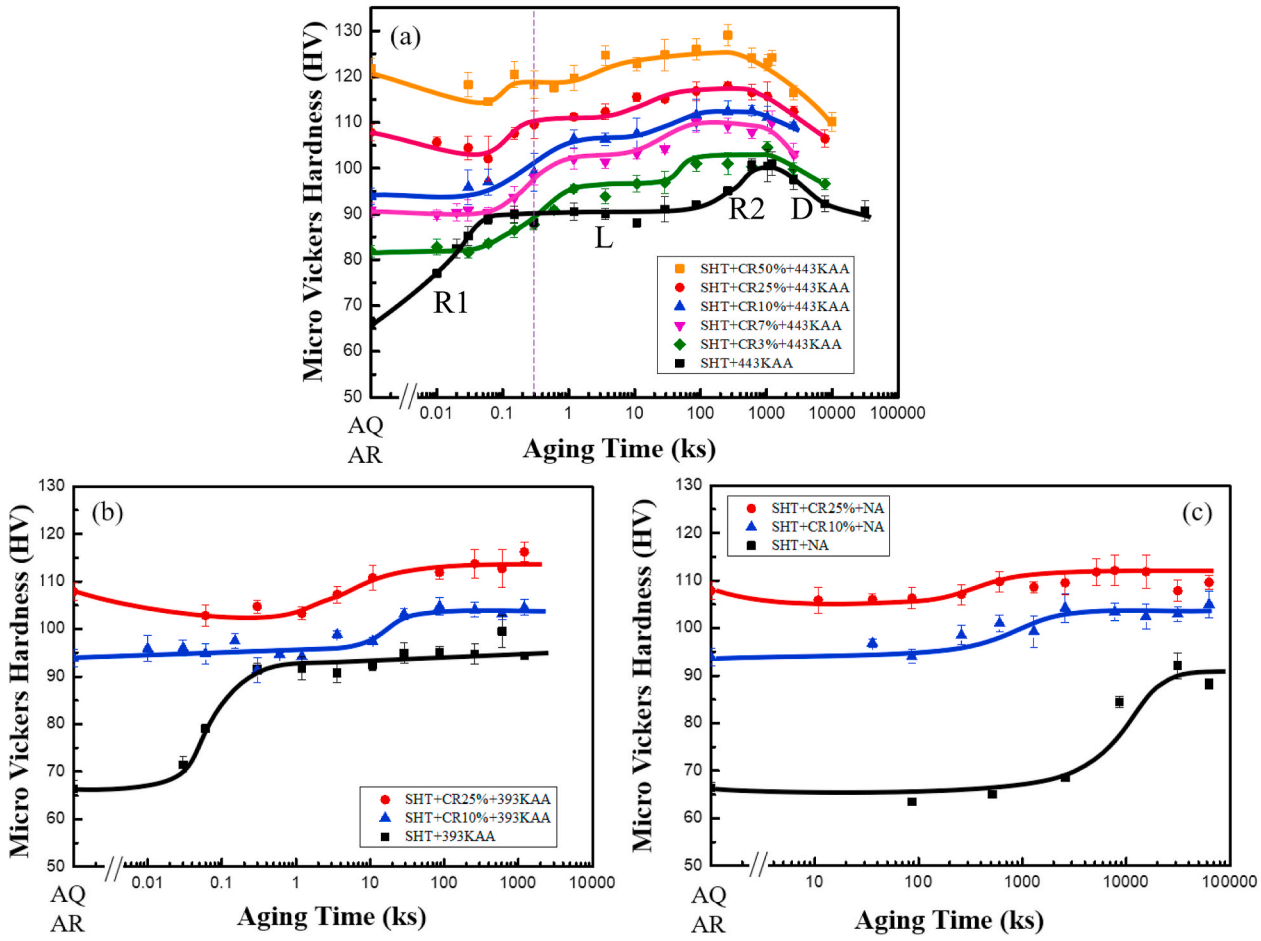

Fig. 2. Age-hardening behavior of the Al-3Mg-1Cu alloy at temperatures (a) 443 K, (b) 393 K, and (c) room temperature (293 K), for various reduction rates. The typical stages in the as-quenched sample are named first rise (R1), plateau level (L), second rise (R2), and decline (D). The labelling indicates the SHT time, CR reduction rate, and subsequent aging temperatures.

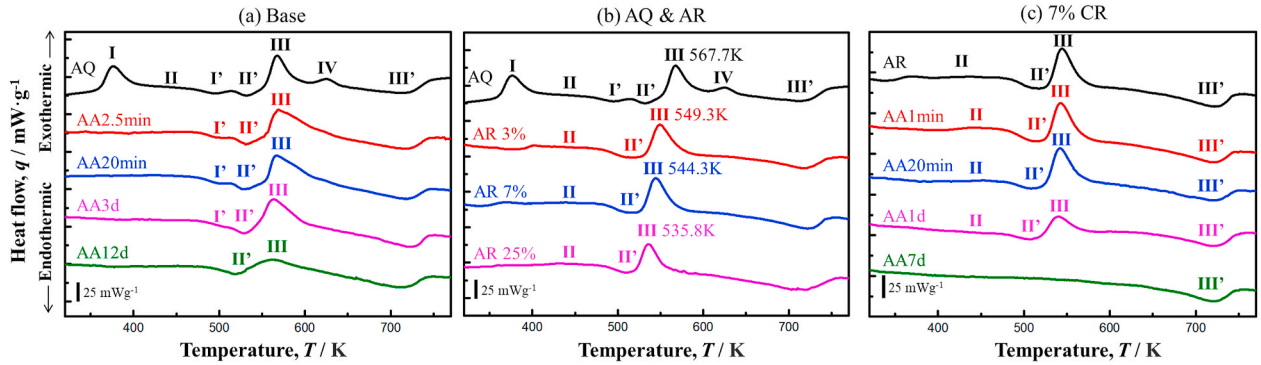

Fig. 3. DSC curves for (a) base alloy aged at 443 K, (b) AQ and AR alloy with various reduction rates, and (c) 7% CR alloy aged at 443 K.

disappears after a short time, which is insufficient to form a precipitate. This peak is not considered in further examination.

3.2.2. *DSC of the as-quenched and as-rolled samples*

The DSC curves of the AQ and AR alloys at different reduction rates are shown in Fig. 3(b). The cluster formation peak I is absent in the AR samples, indicating that the clusters have already been formed, or that they will not form during subsequent aging. The absence of a cluster dissolution peak I' in the AR samples supports the second option, because this means that there are no clusters to dissolve. This is because the dislocations introduced in the CR samples act as vacancy sinks, reducing the fraction of vacancies available for the formation of clusters [33]. This is consistent with the hardness curves of the CR samples without a rapid initial increase in hardness.

We assume that the broad and weak peak II is attributed to the GPB zone formation in the CR samples. The presence of GPB zones is also indicated by the subsequent dissolution peak II'. The temperature related to peak III decreased (567.7 K to 535.8 K) with an increased reduction rate (0 to 25%), indicating that the presence of dislocations may accelerate the formation of the S phase. This is consistent with the hardness curve: the higher the reduction rate, the shorter the time required to reach the peak hardness.

The age-hardening behaviors of the base and CR materials are dominated by different mechanisms. In the base sample, the quenched-in vacancies dominated the diffusion of the solute atoms. This leads to homogenous solute clusters that are responsible for rapid age-hardening. In the CR samples, the deformation-induced dislocations hindered the formation of clusters, instead promoting precipitation on the dislocations. We suggest that this is the reason for the initial hardening stage R1. With more deformation, the dislocations increasingly dominate the diffusion, which results in an accelerated R1 stage as well as a shorter hardness plateau L.

3.2.3. DSC of 7% cold-rolled samples as function of aging time

The DSC curves of the 7% CR samples aged at 443 K for different durations are shown in Fig. 3(c). The DSC curve did not change after aging for 1 min, corresponding to the first incubation stage in the age-hardening behavior. The GPB zone formation peak II nearly disappeared after aging for 20 min, indicating that the GPB zones had already formed. Both the GPB zone dissolution peak II′ and the S phase formation peak III become smaller in the CR samples aged for 1 day, which suggests that a portion of the GPB zones is consumed by the S phases. Only peak III' remained after aging for 7 days. This suggests that the GPB zones do not exist anymore, and the precipitation of the S phases is completed.

3.3. Microstructural characterization

3.3.1. Microstructures in base samples

Fig. 4 (a) and (b) show the HAADF-STEM images of the base samples aged at 443 K for 1 min and 8 h, respectively. The matrix in the sample aged for 1 min contains a high density of small regions of higher contrast (some regions are circled in Fig. 4(a) as examples). This indicates a greater number of clusters. In addition, as indicated by the arrows, some clusters form GPB zones. They grow as short needle-like structures along the <100>Al direction, therefore only the ones viewed in the cross-section have sufficient Cu in the atomic columns to show strong contrast. GPB zones viewed perpendicular to their lengths would contain fewer Cu atoms along the atomic columns and overlap more with the Al matrix. The zones are mostly double eye-like units connected by a distance a_{Al}<210>/2 on a dislocation line [8–10]. This shows that the clusters and GPB zones are responsible for the initial age hardening.

Fig. 4(b) presents an image of the 8 h sample. Here, two S-I plate-shaped precipitates with traces along the <210> Al direction, as visualized by their double Cu layers, have a GPB zone in the middle. This indicates that they were nucleated from the GPB zone. This signifies an S-phase formation that is faster than expected, which corresponds to the plateau stage that represents the "incubation period" for S phase formation [22]. The plates had the smallest possible thickness, indicating a recent formation. This shows that the formation of the S phases can occur before the second hardening stage. This is discussed in Section 3.4, in relation to the dissolution experiments.

3.3.2. Microstructure of cold-rolled samples

Fig. 5 shows the typical HAADF-STEM images of the 7% CR samples after aging for 20 min (a) and 1 day (b-c) at 443 K. After 20 min, the normal GPB zones and GPBX zones, together with thin plates of the S-I phase, formed a continuous band on a dislocation. Normal GPB zones can grow and transform into S-I phases, while the GPBX zones transform into S-II phases upon further aging [9]. This can explain the observation in Fig. 5(b) after aging for 1 day: that two types of S phase predominantly form on the dislocations. The intergrowth of S phases shown in Fig. 5(c) can be explained if the nuclei (normal GPB or GPBX zones) are present on a suitable dislocation line at suitable distances. Evidence of a high density of dislocation lines and loops can be found in the overview of S phases on the dislocations in Figs. S1 and S2 in Supplementary Materials. No precipitates were observed in the AR samples [14].

Combining the results of the hardening curves (Fig. 2(a)), DSC curves (Fig. 3(c)), and TEM analysis (Fig. 5), we conclude that the two hardening stages R1 and R2 in the CR samples correlate with the presence of GPB zones and S phases, respectively.

3.4. Contribution of precipitates to hardness

As mentioned in the previous section, the S phases were found in both the base sample aged for 8 h and the 7% CR sample aged for 20 min at 443 K. However, this may seem inconsistent with the hardening responses. There has been disagreement about whether the GPB zone [24], S phase [31], or a combination [7] are responsible for the peak hardness condition. To elucidate the matter, dissolution experiments for different aging times were performed to evaluate the actual contribution of the GPB zones and S phases to the hardness, for both the base and CR samples.

The samples were heat-treated in a salt bath at each dissolution peak

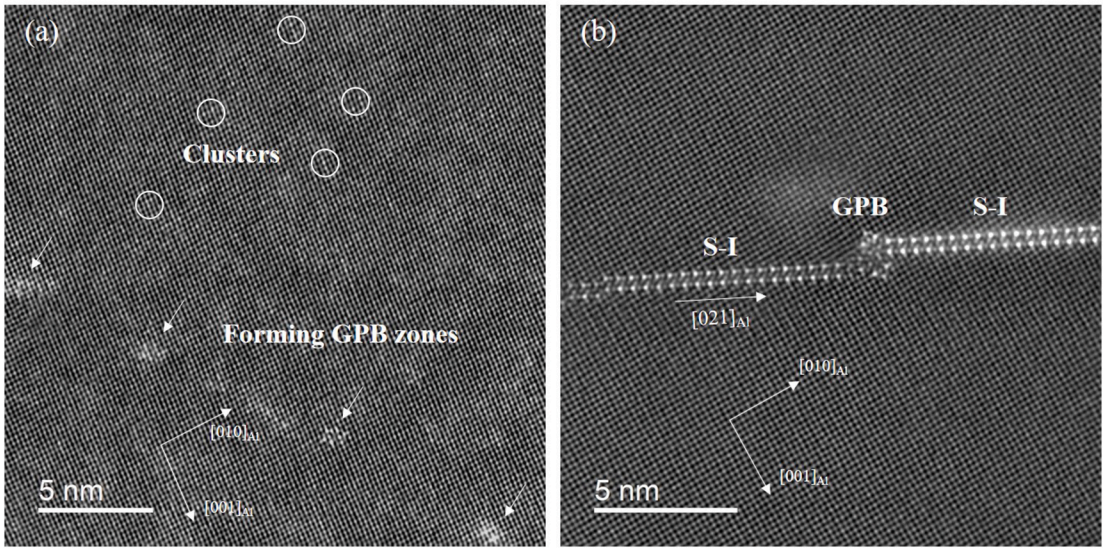

Fig. 4. FFT-filtered HAADF-STEM <100>Al oriented images of the base alloy aged at 443 K for (a) 1min, (b) 8 h. (a) High density of clusters, some clusters are forming into GPB zones. (b) Two precipitates of the S-I phase revealed by their double Cu layers directed along a <210> Al direction, joined by a GPB zone in the center. Notice the rapid contrast variations in the matrix in (a) compared to (b), indicating the high number of clusters in (a).

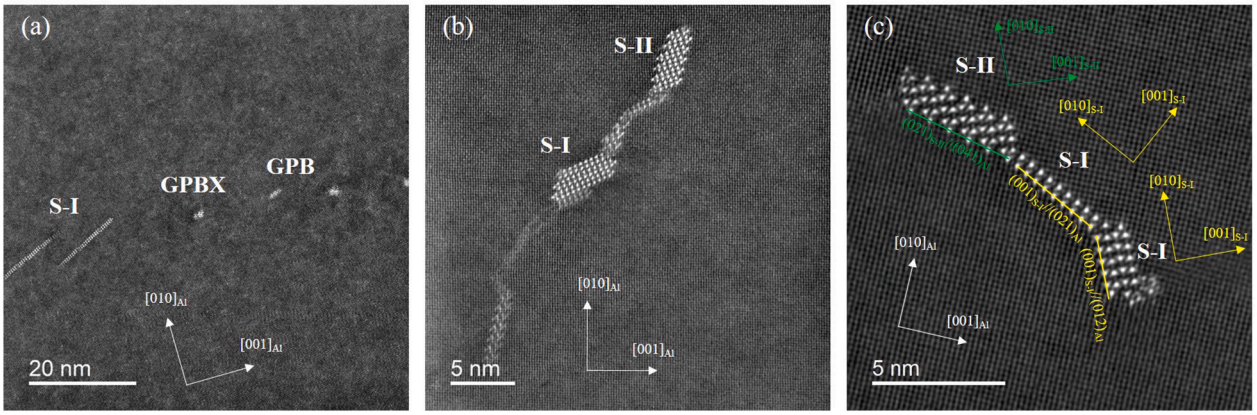

Fig. 5. FFT filtered HAADF-STEM <100>Al oriented images of the 7% CR sample aged at 443 K for (a) 20 min and (b–c) 1 day. (a) Normal GPB zones, a GPBX zone and thin S-I phases located along a dislocation. (b) S-I and S-II phases formed along a dislocation. (c) Intergrowth of S-I and S-II phases.

temperature of GPB zones (531 K, 520 K, 516 K, and 510 K in base, 3%, 7%, and 25% CR samples, respectively) for 2 min to achieve complete dissolution. The hardness reached the maximum value at 2 min of heat treatment and remained almost constant even with further heat treatment. As the dissolution peaks of both the clusters and GPB zones are close to each other, it is difficult to separate them while maintaining accuracy. Both two types of S phases are collectively referred to as S phases because they have the same formation and dissolution peaks and cannot be separated. The loss of hardness after dissolution can be understood as the combined contribution from the clusters and GPB zones. The contribution of S phases to the hardness was obtained by subtracting the contribution of the clusters/GPB zones from the total increase in hardness during aging. The original contribution of the dislocations was determined by the hardness difference before and after cold rolling. The change in the contribution during aging is estimated by referring to the initial stage of age-hardening behavior where no precipitation is formed, and it is assumed that there is no change in the subsequent aging. Therefore, the real drop in hardness due to recovery should be slightly higher than the estimated value. It should also be pointed out that because many S phases are formed along the dislocations, in addition to the individual contribution of the precipitates and the dislocation to the hardness, the interaction between the S phases and the dislocations can also increase the hardness. The contribution of the S phase/dislocation interaction is not shown in the figure because it is difficult to quantify accurately. The interaction can also stabilize the S phases and dislocations, resulting in fewer dislocations being recovered during aging. In this chapter, the contributions of the clusters/GPB zones, S phases, and dislocations to the hardness are discussed.

3.4.1. *Contribution of precipitates to hardness in the base alloy*

The age-hardening responses of the base samples before (black line) and after (green line) the dissolution heat treatment are shown in Fig. 6 (a). The red and blue areas represent the contribution of the clusters/GPB zones and S phases to hardness, respectively, with the values summarized in Table 2. It was found that the increase in hardness in the initial stage of aging was caused entirely by clusters/GPB zones; however, the GPB zones start to dissolve and transform to S phases so that the cluster/GPB zone contribution begins to decrease. The newly nucleated S phase is still small (see Fig. 4(b)) and not significantly different from the GPB zones. Therefore, the dissolved GPB zones and initial small S phases lead to a dynamic balance of the total hardness during the later period of the plateau, which also explains the presence of S phases in the base sample aged for 8 h. With further aging, the S phases begin to grow and increase the hardness until it reaches the peak value where the clusters/GPB zones and S phases contribute to approximately 40% and 60% of the total increase in hardness, respectively. In the over-aging stage, the coarsening of the S phases finally results in a decrease in hardness, while the clusters/GPB zones still almost maintain a certain contribution to the hardness.

3.4.2. *Contribution of precipitates to hardness in cold rolled alloys*

The hardness contribution of the dislocations, clusters/GPB zones, and S phases in the base and CR samples aged at 443 K for various times are shown in Fig. 6(b). The white and orange areas in Fig. 6(b) represent

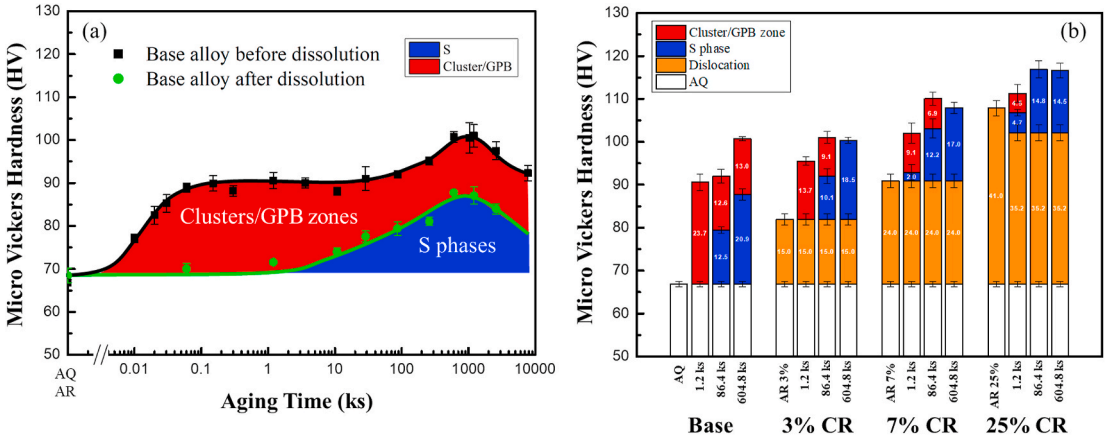

Fig. 6. (a) Hardness curves of aged base alloy before and after dissolution experiments. (b) Hardness contribution of dislocations and precipitates in both base and CR samples.

Table 2
Estimated hardness contribution of cluster/GPB zones and S phases in the base samples as function of aging time.

Aging time	1min	20min	3hr	8hr	1day	3day	7day	14day	30day
	0.06 ks	1.2 ks	10.8 ks	28.8 ks	86.4 ks	259.2 ks	604.8 ks	1209.6 ks	2592 ks
$\Delta HV_{cluster/GPB} = HV_{aged} - HV_{dissolved}$	22.0	23.7	14.1	13.5	12.6	14.0	13.0	13.9	13.5
$\Delta HV_S = HV_{dissolved}$ - HV_{AQ}	–	–	7.1	10.7	12.5	14.2	20.9	20.2	17.1
$\Delta HV_{precipitates} = \Delta HV_{cluster/GPB} + \Delta HV_S$	22.0	23.7	21.2	24.2	25.2	28.3	33.9	34.1	30.6
$\Delta HV_{cluster/GPB} / \Delta HV_{precipitates}$ (%)	100.0	100.0	66.4	55.7	50.2	49.7	38.3	40.8	44.2
$\Delta HV_S / \Delta HV_{precipitates}$ (%)	0.0	0.0	33.6	44.3	49.8	50.3	61.7	59.2	55.8

the intrinsic hardness and the contribution from dislocations, respectively. Note that the red areas in the CR samples are mainly from the GPB zones because almost no clusters are formed during aging, as discussed earlier in section 3.2.2.

We assume that the contribution of the dislocation to hardness does not change during aging in the 3% and 7% CR samples, because no visible recovery is found in their aging responses, as shown in Fig. 2(a). In the 3% CR samples, only the GPB zones were formed after aging for 20 min, while both the GPB zones and S phases coexist in the peak-aged condition. Then, the GPB zones dissolve completely and transform into S phases with further aging. A similar phenomenon was observed in the 7% CR samples, but the S phases were formed after 20 min of aging and contributed more to the peak hardness. Recovery occurred in 25% CR samples. Because dislocation annihilation is significant at the beginning of aging and then weakens to a negligible level, we assume that the contribution of dislocations decreases during the first 20 min, where it tends to stabilize at a certain value. During the aging process, the GPB and S phases coexist at 20 min, and the GPB zones are completely transformed into S phases after 1 day. It was found that the higher the reduction rates, the earlier the S phases were formed. This indicates that dislocations can accelerate the formation of S phases. At the same time, the coarsening stages also advanced due to the dislocations. It is realized that the S phase contribution is lower in the largely deformed samples aged for 7 days, while the high hardness in heavily deformed samples is mainly attributed to the dislocations or the interaction between dislocations and precipitates.

3.5. Tensile test results and fracture surface observations

3.5.1. Tensile properties of the base and CR samples

The stress-strain curves of the base and CR samples aged at 443 K for various times are shown in Fig. 7(a). Their elongation to failure and ultimate tensile stress (UTS) are summarized in Fig. 7(b).

The AQ sample had the lowest yield strength (YS) and UTS, but the highest elongation rate. After 20 min of aging, both the YS and UTS increased significantly while the elongation decreased only slightly, owing to the formation of small and uniform clusters/GPB zones. For the sample aged for 12 days, which corresponds to the peak condition, most GPB zones will have transformed into S phases, resulting in a significant drop in the elongation rate, while the strength is further improved.

After 10% cold rolling was applied, the elongation rate decreased, but YS and UTS increased because of the work hardening effect. The 20 min aged CR sample shows an enhanced strength-plasticity combination (the same YS but both higher UTS and elongation rate) compared to the AR sample, which can be attributed to two reasons: first, a fraction of the dislocations are annihilated during the aging process, causing higher plasticity and greater work hardening tendency (it exhibits a higher increment of stress per strain than the AR sample); second, besides the annihilation of dislocations, solute atoms preferentially accumulate on the remaining dislocations to form GPB zones, a phenomenon which is responsible for the higher strength. With further aging of up to 7 days, the reduction in dislocation density is no longer obvious, and S phases will be formed. The S phases hinder the motion of dislocations, leading to shorter elongation but higher strength.

3.5.2. Fracture surfaces of the base and CR samples

The fracture surfaces of the base and CR samples aged at 443 K for different times are shown in Fig. 8. The fracture surfaces were consistent with the tensile test results. The fracture surfaces of both (a) AQ and (b) 20 min aged base sample contained a large amount of large and deep dimples, which are common in ductile fracture. The fracture surface of (c) the 12 day-aged base sample shows a quasi-cleavage fracture with some dimples, which indicates a more brittle failure mechanism and is consistent with the reduced elongation rate.

The fracture surface of (d) the AR sample shows a quasi-cleavage fracture with only a few dimples, and there are more dimples observed in (e) the 20 min aged CR sample. This indicates that the 20 min aged CR sample has better plasticity than the AR sample. The fracture surface of the (f) the 7 days aged CR sample is a typical quasi-cleavage fracture, which means it is the most brittle sample.

4. Conclusions

The age-hardening behaviors of Al-Mg-Cu alloy, aged with and

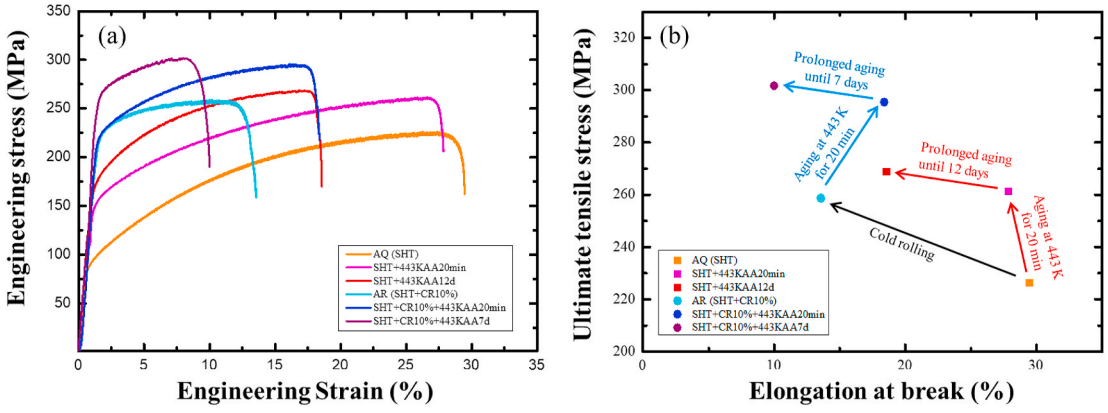

Fig. 7. (a) Engineering stress-strain curves for the base samples and 10% CR samples aged at 443 K for various times. (b) Summary of elongation at the break and ultimate tensile stress of both the base and 10% CR samples.

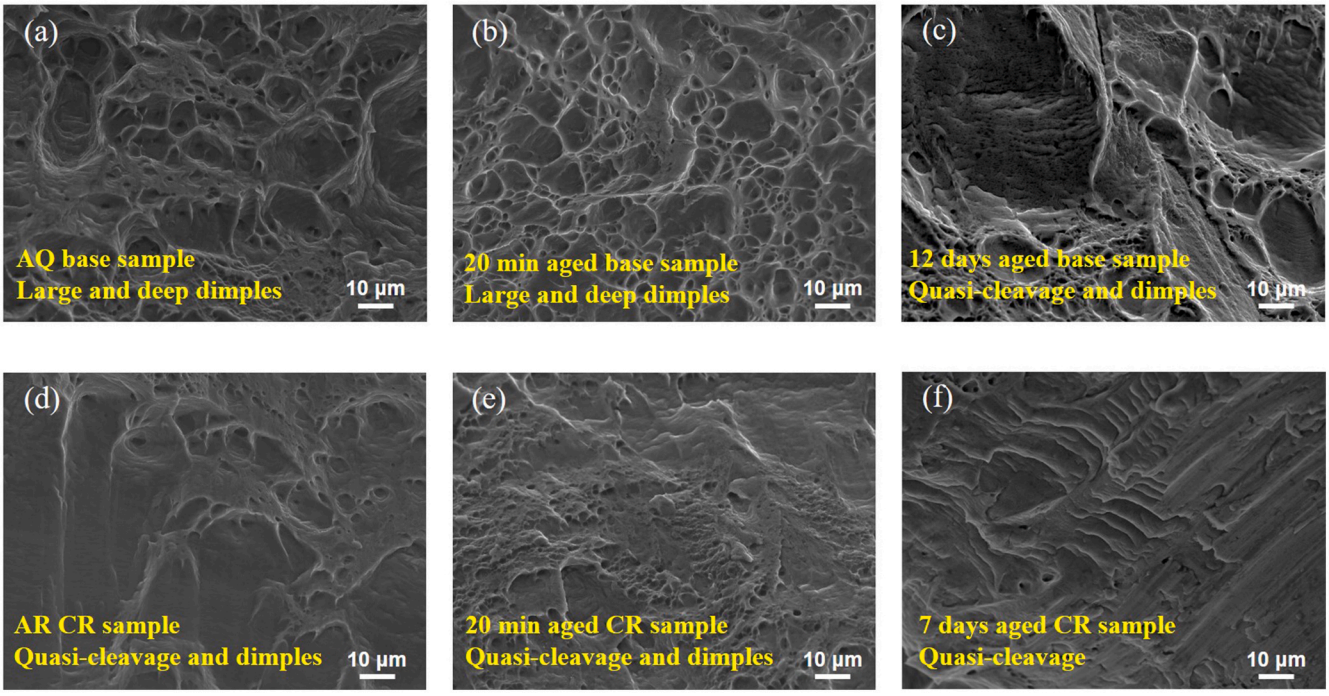

Fig. 8. Fracture surfaces of the base and 10% CR samples aged at 443 K for various times: (a) AQ (b) base, 20 min (c) base, 12 days (d) AR (e) CR, 20 min (f) CR, 7 days.

without pre-deformation in the form of cold rolling, were investigated using hardness measurements, DSC, TEM, tensile testing, and fracture surface observations.

1. Rapid age hardening of the base alloy is absent in CR alloys. Instead, recovery was observed in the highly pre-deformed samples. The hardness peak advances with increasing reduction rate. Aging at low temperatures delays the age-hardening behavior without changing the precipitation mechanism.
2. The near-absence of a cluster formation peak in the DSC curves of the CR alloys indicates that dislocations prevent the formation of clusters. The S phase formation peaks in the DSC curves of the CR alloys appeared at lower temperatures, indicating that dislocations accelerated the formation of S phases.
3. The first increase in hardness in the CR alloys is attributed to the GPB zones because both normal GPB zones and the GPBX zone were observed in the 20 min aged CR samples. Two types of S phases were detected in the CR samples aged for 1 day, suggesting that the second increase in hardness was caused by the S phase formation.
4. The S phases were formed in the later stages of the hardness plateau. The hardness is dynamically balanced by the dissolution of clusters/GPB zones and the formation of S phases.
5. The peak hardness in the base alloy is a combined result of clusters/GPB zones and S phases, and clusters/GPB zones are still stable even after long-term aging. However, contribution of the GPB zones was lower in the CR alloys, and all of them will transform into S phases after long-term aging.
6. When paint-baking (443 K for 20 min) was performed on the as-rolled samples, both the plasticity and strength increased because of the annihilation of dislocations and the formation of GPB zones.

Data availability statement

The raw/processed data required to reproduce these findings cannot be shared at this time, as the data also forms part of an ongoing study.

CRediT authorship contribution statement

Xuanliang Chen: Conceptualization, Methodology, Investigation, Formal analysis, Writing – original draft. **Daehan Kim:** Formal analysis, Writing – review & editing. **Minho O:** Writing – review & editing. **Calin D. Marioara:** Writing – review & editing. **Sigmund J. Andersen:** Writing – review & editing. **Adrian Lervik:** Investigation, Writing – review & editing. **Randi Holmestad:** Funding acquisition, Writing – review & editing. **Equo Kobayashi:** Conceptualization, Funding acquisition, Writing – review & editing, Supervision.

Declaration of competing interest

The authors declare that they have no known competing financial interests or personal relationships that could have appeared to influence the work reported in this paper.

Acknowledgments

The authors acknowledge the INTPART project “Norwegian-Japanese Aluminum Alloy Research and Education Collaboration- phase II” (NFR: 287965) funded by the Norwegian Research Council (NFR) for establishing the collaborations to write this article. This research was also partially supported by the Grant for Integrated Frontier Study, The Light Metals Educational Foundation, Inc., and the SumAl project (294933) from the Norwegian Research Council. The (S)TEM work was carried out on the NORTEM infrastructure (NFR: 197405) at the TEM Gemini Center, Trondheim, Norway.

Appendix A. Supplementary data

Supplementary data to this article can be found online at https://doi.org/10.1016/j.msea.2021.141557.

References

[1] J.C. Williams, E.A. Starke, Progress in structural materials for aerospace systems, Acta Mater. 51 (2003) 5775–5799, https://doi.org/10.1016/j.actamat.2003.08.023.

[2] I.J. Polmear, Light Alloys: from Traditional Alloys to Nanocrystals, Butterworth-Heinemann/Elsevier, Oxford, 2006.

[3] T. Federighi, Quenched-in vacancies and rate of formation of zones in aluminum alloys, Acta Metall. 6 (1958) 379–381, https://doi.org/10.1016/0001-6160(58)90078-6.

[4] P.B. Hirsch, J. Silcox, R.E. Smallman, K.H. Westmacott, Dislocation loops in quenched aluminium, Philos. Mag. A 3 (1958) 897–908, https://doi.org/10.1080/14786435808237028.

[5] Y.A. Bagaryatsk, Structural changes on aging Al-Cu-Mg alloys, Dokl. Akad. SSSR 87 (1952).

[6] A. Charai, T. Walther, C. Alfonso, A.M. Zahra, C.Y. Zahra, Coexistence of clusters, GPB zones, S″-, S′- and S-phases in an Al-0.9% Cu-1.4% Mg alloy, Acta Mater. 48 (2000) 2751–2764, https://doi.org/10.1016/S1359-6454(99)00422-X.

[7] G. Sha, R.K.W. Marceau, X. Gao, B.C. Muddle, S.P. Ringer, Nanostructure of aluminium alloy 2024: segregation, clustering and precipitation processes, Acta Mater. 59 (2011) 1659–1670, https://doi.org/10.1016/j.actamat.2010.11.033.

[8] M. Mihara, C.D. Marioara, S.J. Andersen, R. Holmestad, E. Kobayashi, T. Sato, Precipitation in an Al-Mg-Cu alloy and the effect of a low amount of Ag, Mater. Sci. Eng. A 658 (2016) 91–98, https://doi.org/10.1016/j.msea.2016.01.087.

[9] X. Chen, C.D. Marioara, S.J. Andersen, J. Friis, A. Lervik, R. Holmestad, E. Kobayashi, Precipitation processes and structural evolutions of various GPB zones and two types of S phases in a cold-rolled Al-Mg-Cu alloy, Mater. Des. 199 (2021) 109425, https://doi.org/10.1016/j.matdes.2020.109425.

[10] L. Kovarik, S.A. Court, H.L. Fraser, M.J. Mills, GPB zones and composite GPB/GPBII zones in Al–Cu–Mg alloys, Acta Mater. 56 (2008) 4804–4815, https://doi.org/10.1016/j.actamat.2008.05.042.

[11] L. Kovarik, M.J. Mills, Structural relationship between one-dimensional crystals of Guinier–Preston–Bagaryatsky zones in Al–Cu–Mg alloys, Scripta Mater. 64 (2011) 999–1002, https://doi.org/10.1016/j.scriptamat.2011.01.033.

[12] L. Kovarik, M.J. Mills, Ab initio analysis of Guinier-Preston-Bagaryatsky zone nucleation in Al-Cu-Mg alloys, Acta Mater. 60 (2012) 3861–3872, https://doi.org/10.1016/j.actamat.2012.03.044.

[13] S.B. Wang, Z.R. Liu, S.L. Xia, J. Key, J.H. Chen, Tetragonal-prism-like guinier–preston–bagaryatsky zones in an AlCuMg alloy, Mater. Char. 132 (2017) 139–144, https://doi.org/10.1016/j.matchar.2017.08.014.

[14] X. Chen, C.D. Marioara, S.J. Andersen, J. Friis, A. Lervik, R. Holmestad, E. Kobayashi, Data on atomic structures of precipitates in an Al-Mg-Cu alloy studied by high resolution transmission electron microscopy and first-principles calculations, Data Br 34 (2021) 106748, https://doi.org/10.1016/j.dib.2021.106748.

[15] A.K. Gupta, P. Gaunt, M.C. Chaturvedi, The crystallography and morphology of the S`-phase precipitate in an Al(CuMg) alloy, Philos. Mag. A Phys. Condens. Matter, Struct. Defects Mech. Prop. 55 (1987) 375–387, https://doi.org/10.1080/01418618708209875.

[16] F.J. Niu, J.H. Chen, S.Y. Duan, W.Q. Ming, J.B. Lu, C.L. Wu, Z. Le, The effect of pre-deformation on the precipitation behavior of AlCuMg(Si) alloys with low Cu/Mg ratios, J. Alloys Compd. 823 (2020), https://doi.org/10.1016/j.jallcom.2020.153831.

[17] V. Radmilovic, R. Kilaas, U. Dahmen, G.J. Shiflet, Structure and morphology of S-phase precipitates in aluminum, Acta Mater. 47 (1999) 3987–3997, https://doi.org/10.1016/S1359-6454(99)00259-1.

[18] S.C. Wang, M.J. Starink, Two types of S phase precipitates in Al-Cu-Mg alloys, Acta Mater. 55 (2007) 933–941, https://doi.org/10.1016/j.actamat.2006.09.015.

[19] M.J. Styles, C.R. Hutchinson, Y. Chen, A. Deschamps, T.J. Bastow, The coexistence of two S (Al 2CuMg) phases in Al-Cu-Mg alloys, Acta Mater. 60 (2012) 6940–6951, https://doi.org/10.1016/j.actamat.2012.08.044.

[20] P. Ratchev, B. Verlinden, P. De Smet, P. Van Houtte, Precipitation hardening of anAl–4.2wt% Mg–0.6wt% Cu alloy, Acta Mater. 46 (1998) 3523–3533, https://doi.org/10.1016/S1359-6454(98)00033-0.

[21] P. Ratchev, B. Verlinden, P. De Smet, P. Van Houtte, Artificial ageing of Al-Mg-Cu alloys, Mater. Trans., JIM 40 (1999) 34–41, https://doi.org/10.2320/matertrans1989.40.34.

[22] M. Mihara, E. Kobayashi, T. Sato, Rapid age-hardening behavior of Al-Mg-Cu(-Ag) alloys and incubation stage in the low-temperature aging, Mater. Trans. 54 (2013) 1898–1904, https://doi.org/10.2320/matertrans.MAW201315.

[23] S.P. Ringer, S.K. Caraher, I.J. Polmear, Cluster hardening in an aged Al-Cu-Mg alloy, Scripta Mater. 36 (1997) 517–521, https://doi.org/10.1016/S1359-6462(96)00415-0.

[24] S.P. Ringer, T. Sakurai, I.J. Polmear, Origins of hardening in aged Al-Cu-Mg-(Ag) alloys, Acta Mater. 45 (1997) 3731–3744, https://doi.org/10.1016/S1359-6454(97)00039-6.

[25] A.-M. Zahra, C.Y. Zahra, B. Verlinden, Comments on "Room-temperature precipitation in quenched Al–Cu–Mg alloys: a model for the reaction kinetics and yield-strength development, Phil. Mag. Lett. 86 (2006) 235–242, https://doi.org/10.1080/09500830600678854.

[26] R.K. Gupta, R. Panda, A.K. Mukhopadhyay, V.A. Kumar, P. Sankaravelayutham, K. M. George, Studies on thermo-mechanical treatment of Al alloy AA2219, Met. Sci. Heat Treat. 57 (2015) 350–353, https://doi.org/10.1007/s11041-015-9888-0.

[27] A.K. Mukhopadhyay, R.K. Gupta, K.S. Prasad, P. Sankaravelayutham, Evolution of tensile properties in AA2219 plates due to varying modes and percentages of cold work before artificial aging, J. Mater. Eng. Perform. 29 (2020) 5314–5321, https://doi.org/10.1007/s11665-020-04974-9.

[28] M.M.J. Treacy, Z dependence of electron scattering by single atoms into annular dark-field detectors, Microsc. Microanal. 17 (2011) 847–858, https://doi.org/10.1017/S1431927611012074.

[29] A. Serizawa, S. Hirosawa, T. Sato, Three-Dimensional atom probe characterization of nanoclusters responsible for multistep aging behavior of an Al-Mg-Si alloy, Metall. Mater. Trans. A Phys. Metall. Mater. Sci. 39 (2008) 243–251, https://doi.org/10.1007/s11661-007-9438-5.

[30] M. Mihara, E. Kobayashi, T. Sato, Effect of trace addition of ag on the precipitation behavior of Al-Mg-Cu alloy, Eng. J. 19 (2015) 75–84, https://doi.org/10.4186/ej.2015.19.3.75.

[31] S.C. Wang, M.J. Starink, N. Gao, Precipitation hardening in Al–Cu–Mg alloys revisited, Scripta Mater. 54 (2006) 287–291, https://doi.org/10.1016/j.scriptamat.2005.09.010.

[32] V.A. Esin, L. Briez, M. Sennour, A. Köster, E. Gratiot, J. Crépin, Precipitation-hardness map for Al–Cu–Mg alloy (AA2024-T3), J. Alloys Compd. 854 (2021) 157164, https://doi.org/10.1016/j.jallcom.2020.157164.

[33] T.S. Parel, S.C. Wang, M.J. Starink, Hardening of an Al-Cu-Mg alloy containing Types I and II S phase precipitates, Mater. Des. 31 (2010) S2–S5, https://doi.org/10.1016/j.matdes.2009.12.048.